High-fidelity calculation of modal damping caused by friction at blade roots for single blades and tuned bladed disc assemblies

Article (Accepted Version)

Article type: Material Stress Analysis, Structures

Corresponding author: E.P. Petrov

University of Sussex, Brighton BN1 9QT, United Kingdom, e-mail: y.petrov@sussex.ac.uk

High-fidelity Calculation of Modal Damping Caused by Friction at Blade Roots for Single Blades and Tuned Bladed Disc Assemblies

Junjie Chen[1], Chaoping Zang[1], Biao Zhou[1], E.P. Petrov[2]

[1] Nanjing University of Aeronautics and Astronautics, Aero-engine Thermal Environment and Structure Key Laboratory of Ministry of Industry and Information Technology, Nanjing 210016, China, e-mails: chen_junjie@nuaa.edu.cn; c.zang@nuaa.edu.cn; biao.zhou@nuaa.edu.cn;
[2] University of Sussex, Brighton BN1 9QT, United Kingdom, e-mail: y.petrov@sussex.ac.uk

Abstract

A method for analysis of amplitude-dependent modal damping factors is developed for single blades and tuned bladed discs for the cases when the energy dissipation is caused by the micro-slip motion at friction contacts of blade root joints. Large three-dimensional finite element models and detailed description of friction contacts by surface-to-surface friction contact elements at contact interfaces of the root joints are used for the calculations.

The method allows using available finite element packages and based on the direct calculation of the energy dissipated at root joints for prescribed levels of vibration amplitudes, which takes into account the nonlinear dependency of the modal damping factors on the vibration level.

The numerical studies of the dependency of modal damping factors on the vibration amplitudes are performed for single blades and bladed disc models for different families of modes and nodal diameter numbers.

Keywords

Blade root joints, micro-slip, bladed disc, friction, vibrations, modal damping factors

Introduction

The gas-turbine bladed discs operate under high dynamic loading and high temperatures, and their longevity is usually determined by the levels of vibration and the high cycle fatigue damage caused by the vibration. The effective way to reduce the dynamics stresses are special devices, such as underplatform dampers (see Refs.[1, 2]), or interlock shrouds which allow the reduction of resonance vibration and the shift of the resonance frequencies far from the dangerous operating regimes. The one of the most important sources of the structural damping in bladed disc assemblies is damping in blade root joints. The root damping occurs when the microslip motion occurs at the contact surfaces in blade root and the friction forces dissipate the vibration energy by transferring it to heat. The root damping becomes especially important when, for different reasons, the damping devices is not possible to implement.

There are theoretical and experimental studies of static deformation of root joints with friction contact (see Refs. [3,4]), where the analysis is focused on the distribution and levels of stress and strain in the domains close to the contact surfaces.

There are very restricted number of studies aimed at blade root damping analysis for dynamic response of bladed discs. Among them, the calculations using macro-slip and micro-slip models to simulate the friction are carried out to compare with experimental results in Ref.[5]. The results show that the macro-slip model is appropriate for under-platform damper, while it cannot simulate the interaction of contact surfaces of blade root joints sufficiently well. Different methods are proposed in Refs. [6-11] to simulate the interaction on contact surfaces of blade root joints precisely and to analyse the effect of the root damping on amplitude and resonant frequencies of blade response.

There were several test rigs built for the studies of the root damping in dovetail and fir-tree joints, and experimental measurements of the damping loss factor for different amplitudes, centrifugal forces and mode shapes (see Refs. [12,13]). The relationships between tangential and normal loads of the contact elements are established to solve the dynamic balance functions for blades and disc at the same time in Ref. [14]. The numerical analysis of the effects of friction microslip modelling in root joints using contact elements was made in Ref.[15]. The possibility of prediction of experimentally observed hysteresis loops were studied and insight into effects of different model parameters on micro-slip friction damping properties was obtained.

The quantitative prediction of root damping requires using high fidelity modelling of bladed disc geometry and nonlinear contact interaction in numerical simulations. The model reduction methods is necessary to be perform such simulation in time, which is acceptable in industrial applications. The examples of model reduction techniques aimed and frequency-domain analysis and based on the condensation of the linear parts of the model, while using detailed modelling of contact interfaces are proposed in Ref. [16]

In the paper proposed here the analysis of modal damping produced at the blade-disc joints is investigated. A method is proposed to predict the modal damping

in bladed discs, which is attributed to the microslip motion at blade-disk joints, using large-scale finite element models describing the dynamic properties of the bladed disc components and friction contact interfaces in detail. The method allows the analysis of modal damping for single blades and for bladed disc assemblies. The analysis is performed in time domain by the integrating the equation of motion for a structure with contact interfaces. An original reduction approach is proposed which allows the effective analysis of the structure.

The effect of vibration levels on different vibration modes is studied together with the effects of contact interfaces parameters, such as friction coefficient, contact stiffness coefficients and with effects of the static pre-loading due to bladed disc rotation with different speeds.

Method for Analysis of Friction-Generated Modal Damping

Nonlinear forced response calculation

The equation of motion for a bladed disk with friction contact interfaces can be written in the following general form:

$$\boldsymbol{K}\boldsymbol{x}(t) + \boldsymbol{C}\dot{\boldsymbol{x}}(t) + \boldsymbol{M}\ddot{\boldsymbol{x}}(t) + \boldsymbol{f}(\boldsymbol{x}(t)) = \boldsymbol{p}(t) \tag{3}$$

where $\boldsymbol{K}$, $\boldsymbol{C}$ and $\boldsymbol{M}$ are stiffness, viscous damping and mass matrices of the analysed structure which allow for the pre-stressed effects on the stiffness matrix due to the centrifugal forces and matrix softening effects due to bladed disk rotation; $\boldsymbol{x}(t)$ is a vector of displacements comprising degrees of freedom (DOFs) for all nodes of the finite element model; $\boldsymbol{p}(t)$ is a vector of excitation forces; and $\boldsymbol{f}(\boldsymbol{x}(t))$ is a vector of contact interface forces. The contact interface forces occur due to the interaction between pairing contact surfaces at the blade root contact patches. The contact interface forces are dependent on the relative displacements at the contact interfaces and are highly nonlinear due to: (i) the friction traction stresses and slip-stick transitions during blade vibrations and (ii) the unilateral contact interaction along normal direction to the contact surface.

The method developed in this paper is intended to allow the modal damping assessment using widely available now commercial or free-access finite element codes. Such codes perform the dynamic response calculations for structures with nonlinear forces in time domain mostly, especially when the solutions with strong nonlinearities caused by friction and unilateral contact at blade root contact interfaces are required.

The time domain transient response analysis is performed in this paper with ANSYS Workbench. For the solution of nonlinear contact problems the augmented Lagrange method is chosen, which provides for the considered here problems better robustness and accuracy comparing with the other available algorithms for solution of the nonlinear dynamic problems: the penalty method and the pure Lagrange method.

The modal damping factors characterise the damping properties under steady-state vibrations. Therefore, the time integration applied in the transient response analysis is used to achieve the steady-state vibrations with sufficient accuracy. To achieve the fast convergence of the transient process to the steady-state vibration regime, the structural background damping is introduced. The physical nature of this damping is usually aerodynamic and material damping. The structural damping is introduced by so-called 'beta damping' factors where β is considered to be used to form the damping matrix proportional to the stiffness matrix of the structure: $\boldsymbol{C} = \beta \boldsymbol{K}$.

In the method developed in this paper the modal damping factors are calculated only due to friction damping at the contact interfaces. These factors are determined from the energy dissipated at the contact interfaces and this energy is calculated directly from the work of friction contact forces over period of vibration and over contact interface areas. Owing to this, the choice of the beta damping factor makes usually very little effect on the calculated friction damping at joints. Because of this, the physical damping modelled by beta damping is needed here for the only one reason: to obtain steady-state periodic vibration in accordance with the analysed mode shape when all the other modes are damped. The higher the damping the sooner the steady-state response can be achieved by the transient analysis. However, there is some limit in the choice of the background damping, since too large beta damping values can introduce, for cases when the friction damping is very small, some inaccuracy in the evaluation of the friction-induced energy dissipation.

Moreover, when the transient analysis is performed, all modes of the analysed structure can be excited. For the high fidelity finite element models the low and high natural frequencies can differ very much and the time steps in the transient analysis can become very small in order to capture the very high vibration modes. Yet, such high frequency vibration is irrelevant to the calculation of the modal damping factors for relatively low modes considered in this paper. Because of this, the numerical damping is also introduced to suppress the very high frequency vibration mode capturing during the time integration process.

The extensive studies of effects of the choice of structural and numerical damping values on the accuracy of the friction-generated modal damping has been performed, some examples are shown in this paper below. The tests shows that the value 0.01 can been chosen as the appropriate value for both: (i) the beta damping and (ii) the numerical damping. Using these values provides the efficient and robust search for the steady-state solutions while avoids the introduction of the errors in the calculation of the modal damping caused by the microslip at blade roots even for small friction damping factors.

Reduced modelling in the modal damping analysis

The transient forced response analysis is usually very time-consuming. The bladed disk finite element models conventionally used on the industrial applications can contain from many thousands to millions DOFs. The use of such high-fidelity bladed disk models or even single blade models is not practical due to very large computational expenses. In this paper, an original approach is proposed which allows performing the time domain calculations only for a small part of the structure. The model reduction is based on the assumption, supported by some earlier experiments

and numerical analyses (see e.g. Ref.[8]), that the effect of the root damping on blade mode shapes is small for amplitude levels observed in usual operating gas-turbine engines conditions. In these conditions the microslip friction is prevalent, and for blade nodes located far enough from the friction contact interfaces the modes shape is close to the mode shape determined in the absence of friction. Yet, the energy dissipated by friction, the friction stresses and slip-stick transitions are dependent on the vibration amplitudes and on the local variation of the stress fields at the contact interfaces and near blade root joints. In order to take advantages of these properties of the analysed structure, we suggest using a relatively small part of a whole analysed structure: the part which fully includes all friction contact interfaces of the blade-root joint. The planes which are used to cut the reduced model from the whole structure should be selected far enough from the contact interfaces to have at their surfaces the negligible level of distortion for a considered mode shape. The interaction of the reduced model with the rest of the structure is accounted for by the application of the displacements corresponding to the analysed mode shape at all nodes located at the cutting planes.

The approach proposed here is based, in very general terms, on the Saint-Venant's principle, which states that the displacements and stresses produced in a body by different but statically equivalent systems of loads will differ little at distances comparable with size where these loads are applied. This principle has many fruitful applications and its generality and the rate of decay of the differences with the increase of the distances are discussed in many publications (e.g. see Refs.[20]. and [21].

In the analysis of root damping in bladed discs, the change of contact conditions occurs during vibrations at the blade root contact patches. The size of the modelled root joint model is restricted in circumferential direction by the size of the bladed disc sector, the joint model along the axial direction includes the full bladed disc rim thickness and the size along the radial direction of the model is selected to be proportional to the two other directions. In most cases, the boundaries of the joint model selected by this way are far enough, and the applicability of our approach can be assessed for typical blade root designs by the comparison of natural frequencies and mode shapes at the boundaries of the joint models calculated or measured for different realistic contact conditions: if they do not vary significantly, then this approach is applicable.

It should be noted that the effects of static loading caused mostly by the centrifugal forces are also included in the reduced modelling. The displacements at the boundaries of the considered part are determined from the analysis of the whole structure and then they are applied to the boundary nodes of the reduced model.

To extract the nodal displacements on the boundaries of the reduced model from the results of the static and modal analysis in ANSYS a special APDL code has been developed.

The modal damping for two practical structures are analysed in this paper: (i) a single blade with a root joint and (ii) a tuned bladed disk assembly. Some details of the reduced modelling for these structures are discussed below.

Single blade model reduction

The example of single blade model with a root joint is shown in Figure 1a and its reduced model is shown in Figure 1b. One can see that a part of the disk is included into the model in order to model friction contact interactions at the blade root joint. The reduced model is obtained from the whole model of the blade with root joint by cutting the blade under blade platform and leaving the blade root joint part intact. The blade model shown in Figure 1a contains 8857 solid elements while the reduced model contains 5614 solid elements. Both these models have 896 contact elements distributed over blade root contact areas.

Both model are fixed at the surfaces of the disk part marked by letters B, C, and D in Figure 1b. The static stresses are calculated under action of the centrifugal forces using the whole blade model and then the modal analysis is performed for the blade with fully stuck contact interfaces at blade-disk root joint. For a reduced model, the displacement-controlled boundary conditions are applied at nodes (located on the surface marked by letter A) in the following form:

$$\boldsymbol{x}^A(t) = \boldsymbol{x}^A_{\text{static}} + a\boldsymbol{\phi}^A_j \cos(\omega t) \qquad (1)$$

where $\boldsymbol{x}^A_{\text{static}}$ is a vector of the nodal displacements obtained from the solution of the blade static problem; $\boldsymbol{\phi}^A_j$ is a vector of the nodal displacements corresponding to j-th mode shape, a is the parameter controlling the level of vibration amplitudes; ω is the vibration frequency.

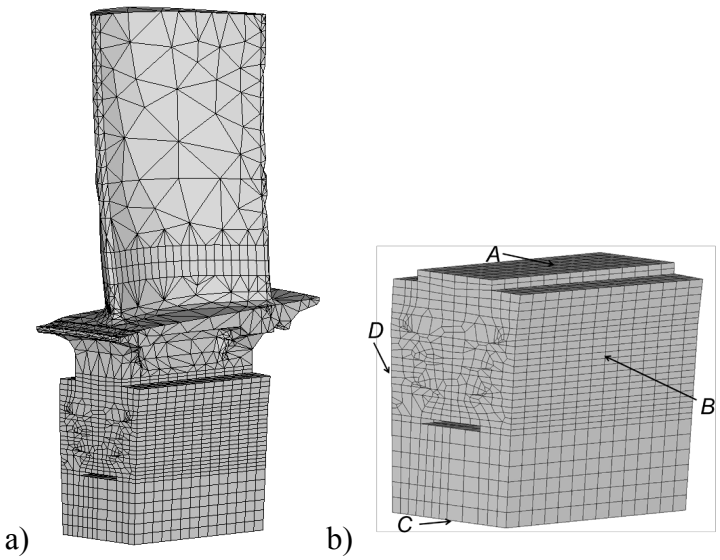

Figure 1. FE models of a) a blade with root joint; d) a reduced model

Tuned bladed disk model reduction

The model of a turbine bladed disc considered here comprises 86 blades unshrouded blades with root joints (see Figure 2a). Owing to the cyclic symmetry of the tuned bladed disks the static and modal analysis can be calculated using its sector model shown in Figure 2b. The analysis of friction-generated modal damping factors is performed using the reduced root joint finite element model shown in Figure 2c. The planes at which the reduced model interacts with the bladed disk are marked by letters A, B, C and D. The finite element model of the bladed disk sector contains

10993 solid elements and the reduced model contains 5614 solid elements and 896 friction contact elements distributed over blade root contact areas.

The analysis of the whole tuned bladed disk can be exactly calculated using only one sector model with the special boundary conditions applied at the planes at which the selected sector is interacting with neighbouring sectors. For the static problem when the loading is due to the centrifugal loading applied identically to all blades the displacements and stresses for all sectors are identical and the boundary conditions reflecting the equality of displacements on left and right sector boundaries: $\boldsymbol{x}_{Right} = \boldsymbol{x}_{Left}$.

For the modal analysis the cyclic symmetry boundary conditions are applied for displacements on the left and right sector boundaries conditions can be expressed in the following form: $\boldsymbol{x}_{Right} = e^{i\frac{2\pi}{N}k}\boldsymbol{x}_{Left}$ where $i = \sqrt{-1}$, N is the number of blades in the bladed disk and k is the cyclic index which is equal to the number of travelling waves along the circumference of a bladed disk. The natural frequencies and modes shapes of bladed disk vibration can be calculated separately for each cyclic index number. The cyclic index can take values from the range 0 - $N/2$ and each j-th mode shape of a cyclically symmetric bladed disk having k travelling waves can be conveniently expressed in the form of complex vectors, $\boldsymbol{\phi}_{jk} = \boldsymbol{\phi}_{jk}^{\mathrm{Re}} + i\boldsymbol{\phi}_{jk}^{\mathrm{Im}}$ in order to describe traveling wave motion excited in gas-turbine engine bladed disks by aerodynamic forces. The mode shapes are complex for all cyclic index values except of cases when $k = 0$ or $N_B/2$. For the latter cases, the imaginary parts of the mode shapes are zero and mode shapes have only real parts, hence they correspond to standing modes of vibrations: for $k = 0$ all blades of a bladed disk vibrate in-phase and for $k = N/2$ blades vibrate in anti-phase. For complex modes shape there are generally phase shifts not only between different bladed disk sectors but also between different points of the same sector.

The displacement-controlled travelling loads are applied at all 4 boundary surfaces of the reduced model by the selection of these nodal displacements from solutions of the static and modal problems obtained for the whole structure:

$$\begin{aligned}
\boldsymbol{x}_{jk}^{A}(t) &= \boldsymbol{x}_{\mathrm{static}}^{A} + a\left[\mathrm{Re}\left(\boldsymbol{\phi}_{jk}^{A}\right)\cos(\omega t) + \mathrm{Im}\left(\boldsymbol{\phi}_{jk}^{A}\right)\cos(\omega t)\right] \\
\boldsymbol{x}_{jk}^{B}(t) &= \boldsymbol{x}_{\mathrm{static}}^{B} + a\left[\mathrm{Re}\left(\boldsymbol{\phi}_{jk}^{B}\right)\cos(\omega t) + \mathrm{Im}\left(\boldsymbol{\phi}_{jk}^{B}\right)\cos(\omega t)\right] \\
\boldsymbol{x}_{jk}^{C}(t) &= \boldsymbol{x}_{\mathrm{static}}^{C} + a\left[\mathrm{Re}\left(\boldsymbol{\phi}_{jk}^{C}\right)\cos(\omega t) + \mathrm{Im}\left(\boldsymbol{\phi}_{jk}^{C}\right)\cos(\omega t)\right] \\
\boldsymbol{x}_{jk}^{D}(t) &= \boldsymbol{x}_{\mathrm{static}}^{D} + a\left[\mathrm{Re}\left(\boldsymbol{\phi}_{jk}^{D}\right)\cos(\omega t) + \mathrm{Im}\left(\boldsymbol{\phi}_{jk}^{D}\right)\cos(\omega t)\right]
\end{aligned} \tag{2}$$

The choice of the travelling wave number, k, and the number of mode , j, is determined by the practical needs of the investigation.

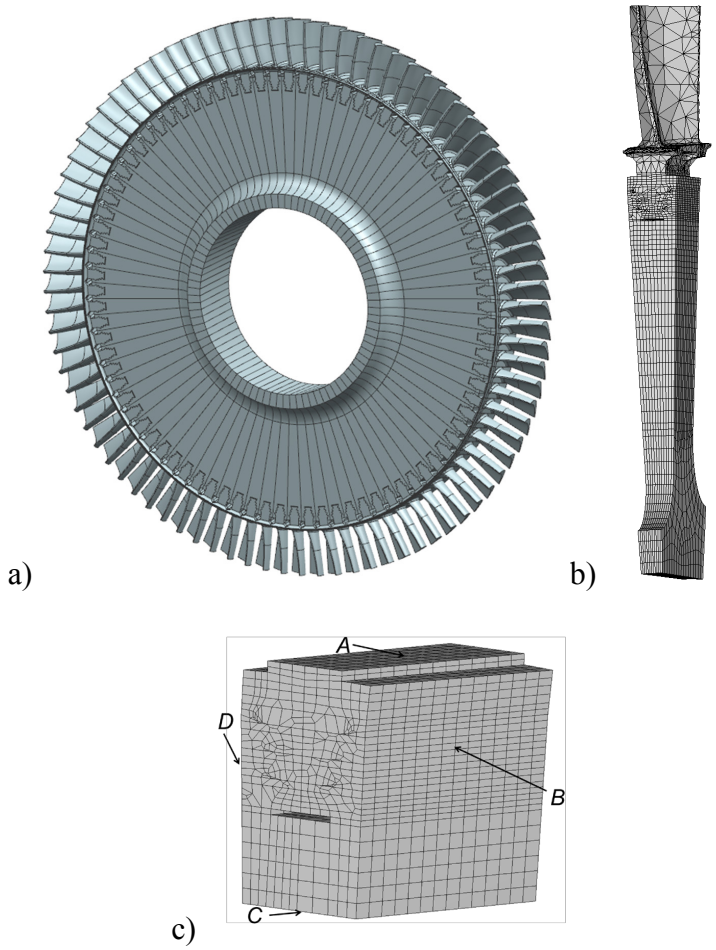

Figure 2. Tuned bladed disk models: a) a bladed disk; b) a sector c) a reduced root joint model

Calculation of the modal damping factors

The friction contact interaction modelling

For friction contact modelling at root joints, the surface-to-surface 4-node contact elements are applied over all contact patches of a blade root joint to describe the contact interaction including the friction forces occurring between two pairing contact surfaces. The contact elements use the regularised Coulomb friction model. When the tangential stress exceeds the friction stress limit, the contact point is slipping and the friction stresses are equal to friction stress limit, otherwise it is stuck and the traction contact forces are defined by the relative displacements and the tangential contact stiffness coefficient. The friction traction stresses, τ ,at contact nodes during the slip state are expressed as:

$$\tau(t) = -sign(\dot{x}^{\tau}_{rel}(t))\mu\sigma_n(t) \tag{3}$$

where μ is friction coefficient; $\sigma_n(t)$ is the normal stress applied at the considered point of the contact surface and $\dot{x}^{\tau}_{rel}(t)$ is the projection of the relative velocity of pairing contact nodes to the contact surface.

For the stuck state at a contact node, the traction stress is determined from the elastic deformation of the contacting rough surfaces, it is expressed through the relative tangential displacement, $x_{rel}^{\tau}(t)$, in the form:

$$\tau(t) = k_t x_{rel}^{\tau}(t) \tag{4}$$

where k_t is the tangential stiffness coefficient. The contact stiffness coefficients describe the contact stiffness caused by the layer of microscopic asperities. The micro asperities are due to inherent roughness of all realistic contact surfaces and the stiffness coefficients are provided per a unit contact area (see Refs.[18] and [19]).

The normal stress, $\sigma_n(t)$, modelling takes into account the unilateral interaction of the contact surfaces when stresses are occur only when gaps are closed and only compressed total stresses can be transferred, i.e.

$$\sigma_n(t) = \begin{cases} 0, \text{ for } k_n x_{rel}^{n}(t) + \sigma_n^{static} \le 0 \\ k_n x_{rel}^{n}(t) + \sigma_n^{static}, \; otherwise \end{cases} \tag{5}$$

where k_n is the normal contact stiffness, $x_{rel}^{n}(t)$ is the relative displacement of the contacting surfaces along normal direction to the contact interface and σ_n^{static} is the static component of the normal stresses.

The major friction interface parameters used in the friction contact modelling (the friction coefficient together tangential and normal contact stiffness coefficients) are dependent on material properties of the contacting elastic bodies, on the surface finish and resulting from this roughness, the temperature at which the contact interfaces operate, etc. Usually these parameters are determined from experimental measurements (see e.g. Ref.[17]).

Calculation of the energy dissipated by friction forces

The energy dissipated by friction forces at root contact interfaces over a vibration period is calculated by direct evaluation of the work of the friction forces on the relative displacements over areas of all contact interfaces:

$$W = \int_0^{2\pi/\omega} \left[\sum_{j=1}^{n_A} \int_{A_j} \tau(\xi,\eta,t)\, \dot{x}_{rel}^{\tau}(\xi,\eta,t)\, dA \right] dt \tag{6}$$

where A_j is area of j-th contact patch at the blade root joint and ξ and η are coordinates of the nodes in the local coordinate system of a contact patch. The friction stress and relative displacement values are selected for all nodal values at the contact interfaces from the time-domain solution obtained in a result of the transient analysis performed for the reduced model. This selection is performed for uniformly time-spaced points over a single cycle of the vibration when the time-domain solution becomes sufficiently close to periodic vibration. The selection is performed using the developed APDL code. A specially created MATLAB code is then used to manage

these data and to calculate energy dissipated at contact interfaces. The numerical integration of Eq.(6) is performed and the Gaussian quadrature formula is used to perform the integration of the dissipated energy within each contact interface element. The formula used for the evaluation of the energy dissipated over one period takes the form:

$$W = \sum_{k=1}^{n_t} \sum_{j=1}^{n_E} \sum_{i=1}^{n_G} w_i \tau_j \left(\xi_i, \eta_i, t_k\right) \left[x_{rel}^{\tau} \left(\xi_i, \eta_i, t_k\right) - x_{rel}^{\tau} \left(\xi_i, \eta_i, t_{k-1}\right) \right] A_j \tag{7}$$

where n_E is the total number of contact interface elements all contact interface patches; n_G is the number of Gaussian integration point used for each contact element – 4 points are used in our calculations; n_t is the number of time steps over one period used for the dissipation energy evaluation; A_j is area of j-th contact element; w_i is the weight coefficient value at i-th Gaussian quadrature point; and $\tau_j \left(\xi_i, \eta_i, t_k\right)$ and $x_{rel}^{\tau} \left(\xi_i, \eta_i, t_k\right)$ are values of friction stresses and relative displacements calculated at specified time instants and locations.

Calculation of the modal damping factors

The damping factor is calculated from one of the definitions of the modal damping: using the ratio of the dissipated energy and the maximum strain energy, for the considered level of vibrations, when the analysed system performs vibrations accordingly to the mode shape analysed, $\boldsymbol{\phi}_{jk}$, with the prescribed level of amplitude, a . The amplitude level is controlled in our calculations by the magnitude of the amplitude vector at the blade tip at the outlet edge of the blade airfoil. The calculated mode shapes, $\boldsymbol{\phi}_{jk}$, are mass-normalised and the blade strain energy for the whole structure vibrated at the required level, a , can be obtained as:

$$E_{jk}\left(a\right) = \frac{1}{2} \left(a\boldsymbol{\phi}_{jk}^{H}\right) \boldsymbol{K} \left(a\boldsymbol{\phi}_{jk}\right) = \frac{1}{2} a^2 \omega_{jk}^2 \tag{8}$$

where ω_{jk} is the natural frequency of the considered mode. Then the modal damping factor, η_j , calculated for mode shape $\boldsymbol{\phi}_{jk}$ with the blade tip vibrating at amplitude, a , is determined from the following formula:

$$\eta_{jk}\left(a\right) = W_{jk}\left(a\right) \Big/ \left(2\pi E_{jk}\right) = W_{jk}\left(a\right) \Big/ \left(\pi a^2 \omega_{jk}^2\right) \tag{8}$$

where $W_{jk}\left(a\right)$ is the dissipated energy calculated using Eq.(7) for a mode $\boldsymbol{\phi}_{jk}$.

Numerical studies of the modal damping

The examples of the modal damping factor studies are presented in this section for three models of blades with root joints.

First model is a simplified blade root model, which is used to explore the numerical properties of the calculation procedures, the effects of the contact interface

parameters and finite element mesh size and for some verification of the reduced modelling method proposed here.

Two other models are: (i) a single realistic blade with root joint and (ii) a tuned bladed disc. These models were built to investigate how mode shapes and vibration levels affect the modal damping factor caused by microslip at blade root contact surfaces in condition close to operating conditions. Effects of rotating speed, friction coefficient, tangential contact stiffness on the damping factor are assessed.

In all these models, the normal and tangential contact stiffness coefficients are assumed $k_n = k_t = 10^5 N/mm^3$, and the friction coefficient is $\mu = 0.4$, if other values are not specially specified. The operating rotating speed 1000 rad/s is applied for the calculation of static displacement and stress levels caused by the centrifugal forces.

A simplified blade with root joint

The finite element model of the simplified blade is shown in Figure 3. The blade model with root joint contains 4004 solid three-dimensional elements. There are two contact surfaces at both sides of the blade root and from 78 to 390 contact elements are applied at each of these surfaces – depending on the study performed and the accuracy requirements.

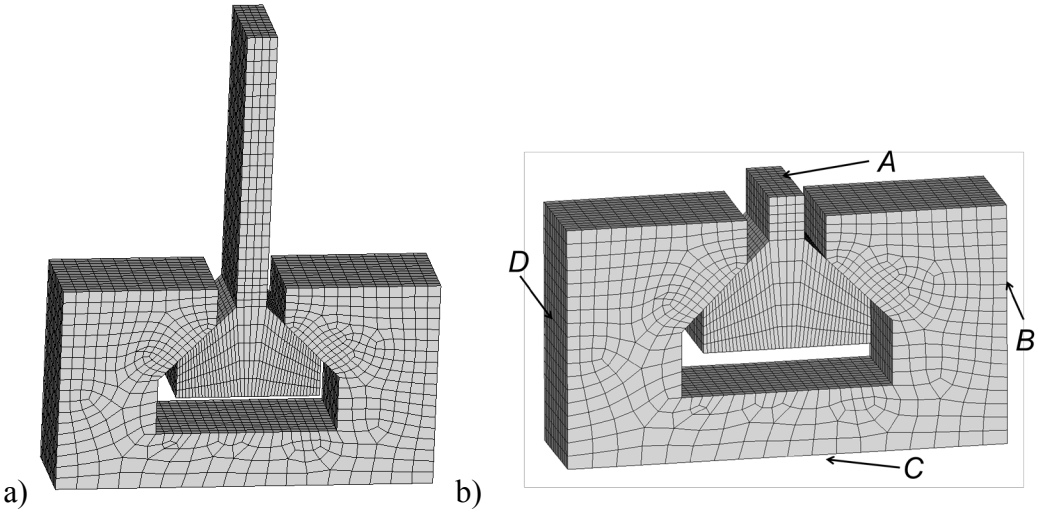

Figure 3. FE models of a) a simplified blade with root joint; d) a reduced root joint model

For the simplified blade root model, first four mode shapes are analysed: 1st flap (1F), 1st edge-wise (1E), 1st torsional (1T) and 2nd flap (2F) modes. The calculated mode shapes for the considered model are shown in Figure 4.

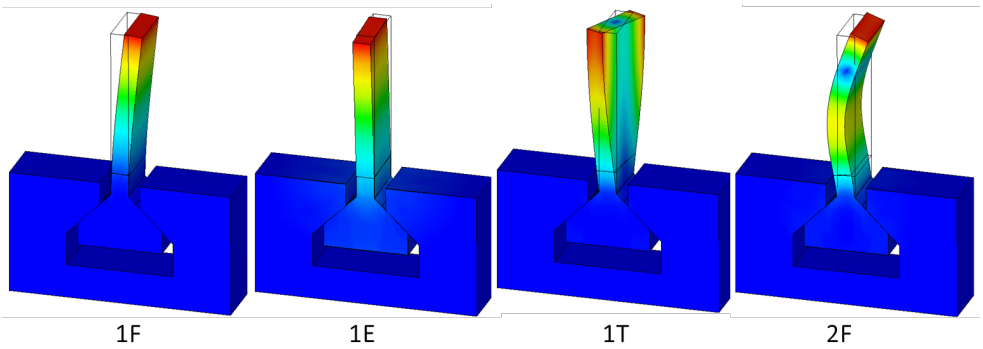

Figure 4. Four mode shapes of the simple model

The choice of time-domain integration parameters for transient response calculation

The influence of beta damping and numerical damping has been assessed thoroughly at the beginning. The example of the calculation results of damping factor caused by friction for different values of numerical and beta damping are plotted in Figure 5 for all modes with the tip amplitude value 0.5mm. From these plots, we can see that for all modes (except of 1F mode) the choice of values for beta damping and numerical damping does not affect much the calculated modal damping factors. This happens, since the friction damping provides the relatively high modal damping factor, which overcome the small effect of these damping factors. However, the modal damping for 1F mode is very small ~10^{-6} and for this case the beta damping and numerical damping can introduce some errors by increasing the values of modal damping factor: due to introducing spurious phase shift between contact loads and displacements. Generally, very high values of numerical and beta damping can affect the values of the calculated modal damping when the friction damping is very low. The appropriate choice of these parameters allows the accurate estimate of modal damping caused by friction for practical ranges of their values. They cannot be set to be equal to zero since the transient process is needed to converge to the steady-state periodic vibration and we want to ensure fast enough convergence of the transient response to steady-state vibration. However, the beta damping and numerical damping should not be chosen too large – to allow the accurate prediction of the friction-induced modal damping. The analysis performed has shown that the values for beta and numerical damping 0.01 can be a good choice for predictive analysis of the modal damping using the methodology proposed in this paper.

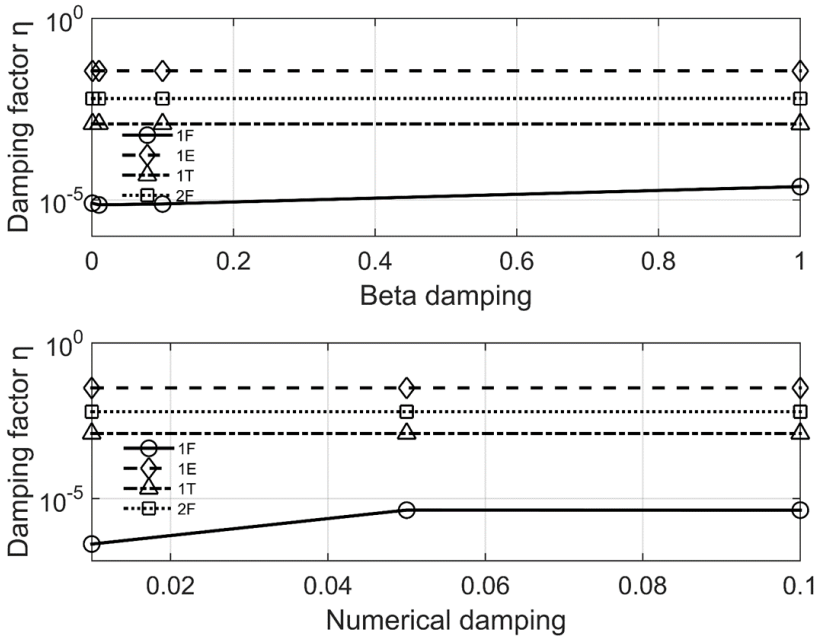

Figure 5. Effect of the numerical and beta damping values on the modal damping

The choice of the number of cycles necessary for the convergence of the energy dissipated at contact interfaces over a vibration cycle has been analysed also. In Figure 6 an example of the evolutions of the dissipated energy with the vibration cycle number are shown for 1E mode: the case are considered when the amplitude levels at blade tip are: 0.3, 0.5 and 0.7mm. We can see that the energy dissipation converges rather quickly here: the dissipation energy is stabilised after several vibration periods. As expected, the dissipated energy stabilisation is achieved faster for structures with higher amplitudes because they have higher friction damping levels.

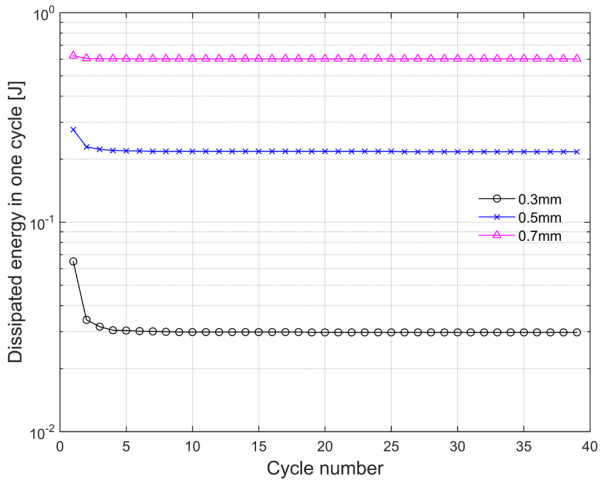

Figure 6. Variation of the energy dissipation with vibration cycle numbers

The effect of the number of contact elements used for the modelling of contact interactions is demonstrated in Figure 7 where the hysteresis loops are plotted for the friction forces calculated over contact surface on the right side of the simplified blade root. The relative displacement for these plots is calculated in the middle of the contact surface. The number of contact elements on each side of the simplified blade model used in the calculations are 78, 104, 182 and 390. It is evident that all these hysteresis loops are very close, especially if we compare the area of the hysteresis loops. The latter is the defining characteristic in the modal damping calculation since the hysteresis loop area is proportional to the energy dissipated over one period. Moreover, 78 elements are sufficient to obtain the convergence not only for the area but also for the hysteresis loop shape. The effect of the contact element size and their number on the calculated damping factors values is demonstrated in Figure 8. It is evident that the increase of the number of elements from 78 to 390 changes the modal damping factor value not significantly: by ~5%. More comprehensive analysis of the effects of mesh quality and other modelling parameters can be found in Ref.[15]

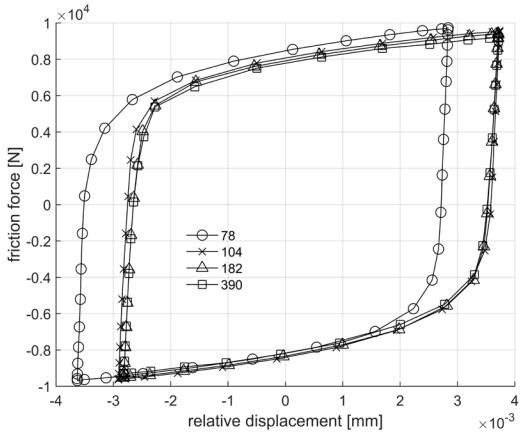

Figure 7. Effect of the number of contact elements on hysteresis loops (at right contact interface of the root joint)

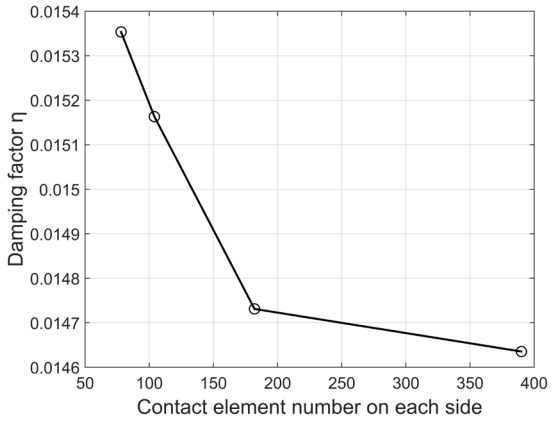

Figure 8. Effect number of the contact interface elements on the modal damping factor

The effect of vibration amplitude

The friction contact interactions at blade root has essentially nonlinear character and the variation of the damping factor with the increase of the vibration amplitude level is shown in Figure 9. The modal damping is studied for four first blade mode shapes. The damping factors differ significantly for different modes and the damping factor

value for 1F mode is much smaller than for the other modes considered here. To compare the variation of the damping factor for this mode together with results obtained for the other modes in the same plot, the modal damping factor values obtained for 1F mode are multiplied in the plot by factor 5. The results plotted in this figure are obtained for two different contact interface element meshes: (i) when 78 contact elements are applied at each of two contact patches and (ii) a case when 182 contact elements are used. It is evident that the damping factor does not differ significantly and the use of 78 contact elements is sufficient for all amplitude levels analysed here

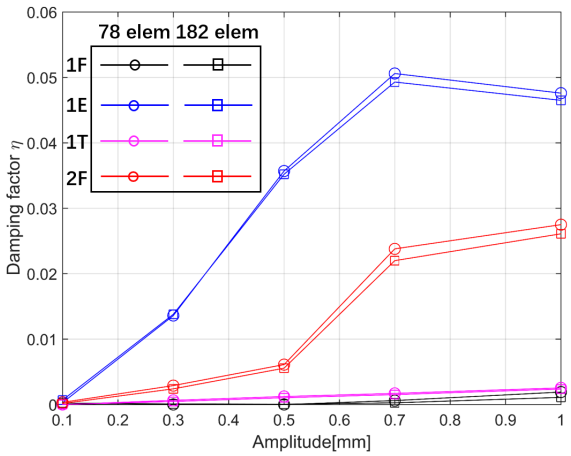

Figure 9. The variation of the damping factor with amplitude increase

With the amplitude increase, the damping factor has a tendency to increase at first for all considered modes: when the amplitude levels are small. For 1F and 1T modes, the damping factor increases slowly. The values of damping factor for these two modes are much smaller than for 1E and 2F modes with the same level of vibration amplitudes at blade tip. The dependency of modal damping factor on the vibration amplitude is monotonically increasing for 1F, 1T and 2F modes, although for 1E mode produces the largest modal damping factor, which increases at first then reaches its maximum at amplitude level 0.7mm and under further increase of the amplitude it starts to decrease. This behaviour can be explained by the behaviour of the friction contact interfaces at blade roots: at very small vibration levels, the static contact pressure caused by the centrifugal forces prevents the slip at contact interfaces and the energy dissipated by friction is close to zero. With the growth of vibration amplitude, the slip occurs over larger and larger contact area and the energy dissipated by friction forces increases and therefore the damping factor grows. After achieving some threshold, the further amplitude increase does not increase the slipping areas significantly while the strain energy starts to grow faster than the energy dissipated by friction. As a result, the decrease of the modal damping factors is observed for 1E mode for higher amplitude levels. The amplitude level at which the further increase of the amplitude starts to decrease the modal damping factors is different for different modes and for the other modes analysed here it is not reached yet. The values of this amplitude threshold is dependent on the mode shape and, hence, on the ratio between the stresses at the root joint and blade tip amplitude, which is used in our studies as a parameter controlling the vibration level. Moreover, the static loading and friction contact interface parameters, such as friction coefficient and contact stiffness coefficients are also influential here

The effect of rotating speed

The normal pressures acting on the contact surfaces in bladed disks are defined by the centrifugal forces, which are proportional to the second order of the rotating speed. The increase of the rotating speed increases the normal load at the contact surfaces. Moreover, the rotation speed and pre-stressed effects caused by the centrifugal forces affect the natural frequencies and mode shape of blades. The effect of the rotation speed increase can be different for different amplitudes, modes and contact parameters. The effects of the rotation speed on the calculated modal damping have been studied and an example of the dependency of the modal damping factor on the rotation speed are shown in Figure 10 for different modes. To check the mesh convergence for different rotation speeds, the calculations are performed for two different contact interface finite element meshes: with 78 and with 182 elements at each contact patch. Both meshes provide very similar results. The blade tip vibration amplitude for is kept constant for all cases plotted here and set to 0.5mm and the static loading is varied by variation of the rotation speed: modal damping for cases of 300, 500 and 1000 rad/s are calculated.

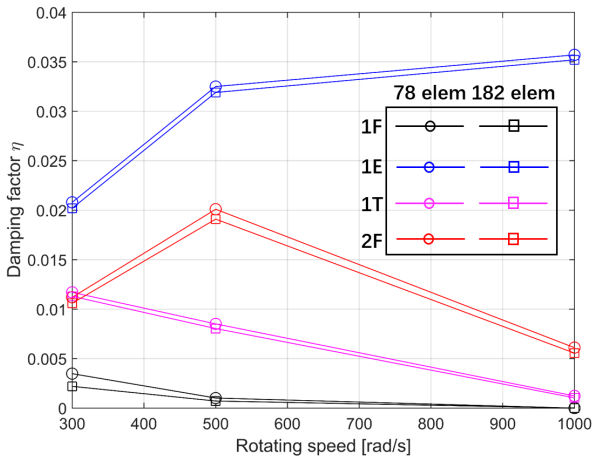

Figure 10. Effect of the rotating speed variation on the modal damping factor

The curves in Figure 10 show different trends for the considered mode shapes in the rotating speed range from 300 to 1000 rad/s. In the assessment of these curves we need to take into account that they are just one part of the whole changing curve for damping factor with respect to the rotating speed.. One can see in Figure 10, that increase of the rotation speed and corresponding increase of the normal pressures decreases the modal damping factors for 1F and 1T modes over the whole rotation frequency range analysed. This is owing to the fact that, for these modes a relatively small part of the contact area is subjected to slip, and the increase of the normal pressure decreases here the slipping areas and slipping distances and hence the dissipated energy is decreased together with the modal damping. For mode 2F increase of the rotation speed from 300 to 500 rad/s increases the dissipated energy by increasing the friction stress limit, $\mu\sigma_n$ (where μ is friction coefficient and σ_n is the normal pressure) on slipping parts of the contact interface and therefore increasing the modal damping at the beginning. However, the further rotation speed increase decreases the contact areas where slip can occur and the modal damping factor starts to decrease. For mode 1E the increase of the modal damping is observed for the whole range of rotation speed variation, although the rate of increase is gradually decreasing

and we can expect that the root damping will start to decrease with further increase of the rotation speed.

We can also conclude that, similar to tuning the underplatform dampers for each mode shape and vibration amplitude level, there rotating speed exists which can provide the largest damping factor for the blade root energy dissipation. Therefore, the blade root should be also designed to provide the maximum root damping at a desired rotor rotation speed.

The effect of the size of reduced blade-disk joint model

The effect of the size of the reduced bladed root models in the analysis of the root damping is checked using the simplified blade root models of different size shown in Figure 11.

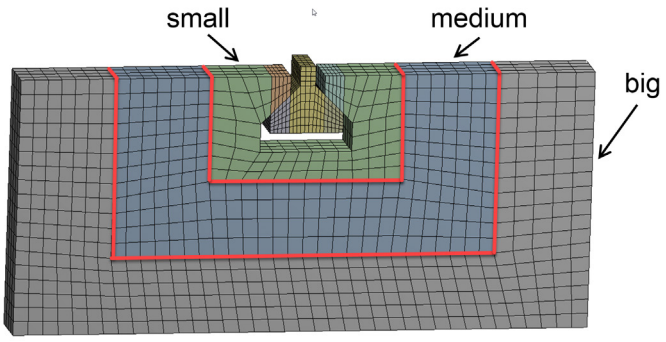

Figure 11. The finite element models of different size used for the method verification

Three different reduced models are explored here: (i) a big model, which includes all finite elements of the plate used for the modelling of the disk. The boundaries of this model are fixed and the displacement-controlled excitation is applied over the surface where the blade is attached to the blade root; (ii) a medium model and (iii) a small model. For the medium and small models, the boundary conditions at the surfaces where these models are cut from the big model are used, in accordance with the method developed, as the displacement-controlled excitation with the displacement distributions defined by the mode shape calculated for the big model. The damping factors are calculated for the blade tip amplitudes: 0.01mm, 0.1mm and 0.5mm. The values of normal and tangential contact stiffness coefficients are $k_n = k_t = 10^5 N/mm^3$, and friction coefficient is $\mu = 0.4$. The static loading corresponding to rotating speed 1000rad/s is applied.

The damping factor values calculated using these different size models are shown in Figure 12. In the considered vibration amplitude range, the damping factor increases with the tip amplitude. There are some discrepancies in the damping factor values obtained with models considered here. However, these discrepancies are sufficiently small, which confirms that the applicability of the proposed model reduction method.

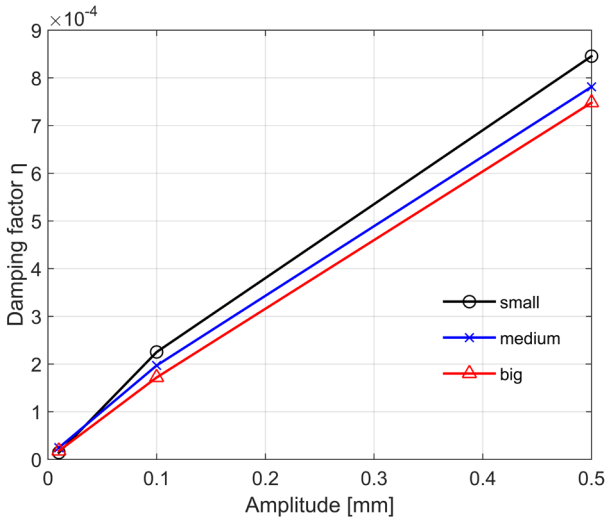

Figure 12. The modal damping factor dependency on the amplitude obtained with different models

A realistic single blade

The studies of modal damping factors caused by friction at blade root joints has been also investigated. The finite element model of the blade and the reduced model are shown in Figure 1. The first four mode shapes for the single blade realistic blade root model are studied. Similar to the case of the simplified blade model considered above, 1F, 1E, 1T and 2F modes are studied. The blade mode shapes are shown in Figure 13. The rotation speed value in realistic operating conditions is applied in the analysis.

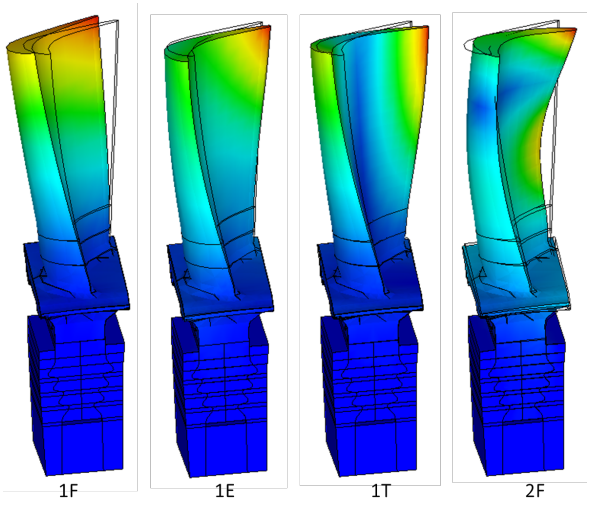

Figure 13. Four mode shapes of the single blade realistic model

Effect of vibration amplitude

The considered range of the blade amplitude variation is chosen here from 0.01 to 1mm. The normal and tangential contact stiffness are $k_n = k_t = 10^5 N/mm^3$, and the friction coefficient is $\mu = 0.4$. The curves of damping factor variation as a function on the blade amplitude for four mode shapes are shown in Figure 14. In contrast to the case of the simplified blade model, all modes have here curves with the local maximum. The modal damping curves increase with the amplitude increase at first,

reach their maximum values (which are different for different mode shapes), and then start to decrease with the further amplitude increase. Similar to the results obtained for SBRM, the value of damping factor for 1E and 2F are significantly bigger than for 1F and 1T, although the difference is not as prominent as before.

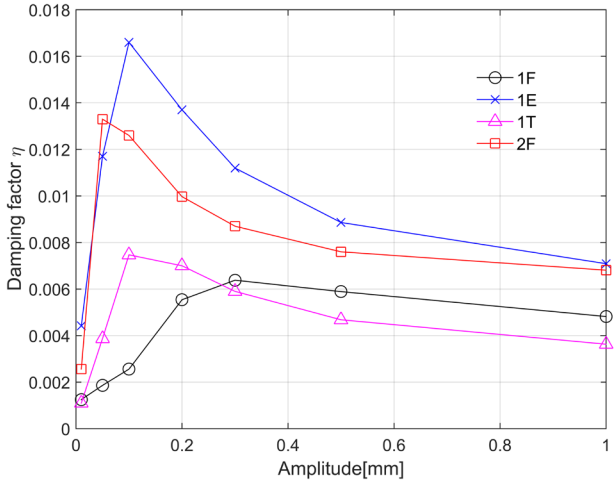

Figure 14. Modal damping factor dependency on the vibration amplitude

It should be noted that for all these calculations the transient response converged to the steady-state calculation fast and the example of variation of the dissipated energy power over analysed vibration cycles are shown in Figure 15, for a case of 1E mode. One can see that the dissipated power is in steady state regimes for the considered vibration amplitudes. For the calculation of the dissipation energy details of the friction stress and relative displacement distributions over contact surfaces are accounted for. Two examples illustrating the complex variation of the contact over all contact surfaces are shown in Figure 16 for 1E and 2F modes. Here, the contact status variation over period is plotted for all nodes: stick, slip or separation; The status is shown for 6 equally-distanced time instants chosen over the half of the vibration period, T .

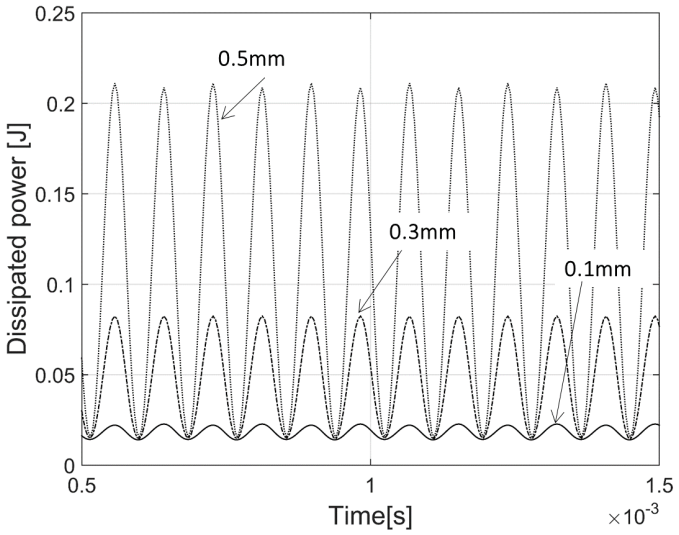

Figure 15. Variation of the dissipation energy power over vibration cycles: a case of 1E mode

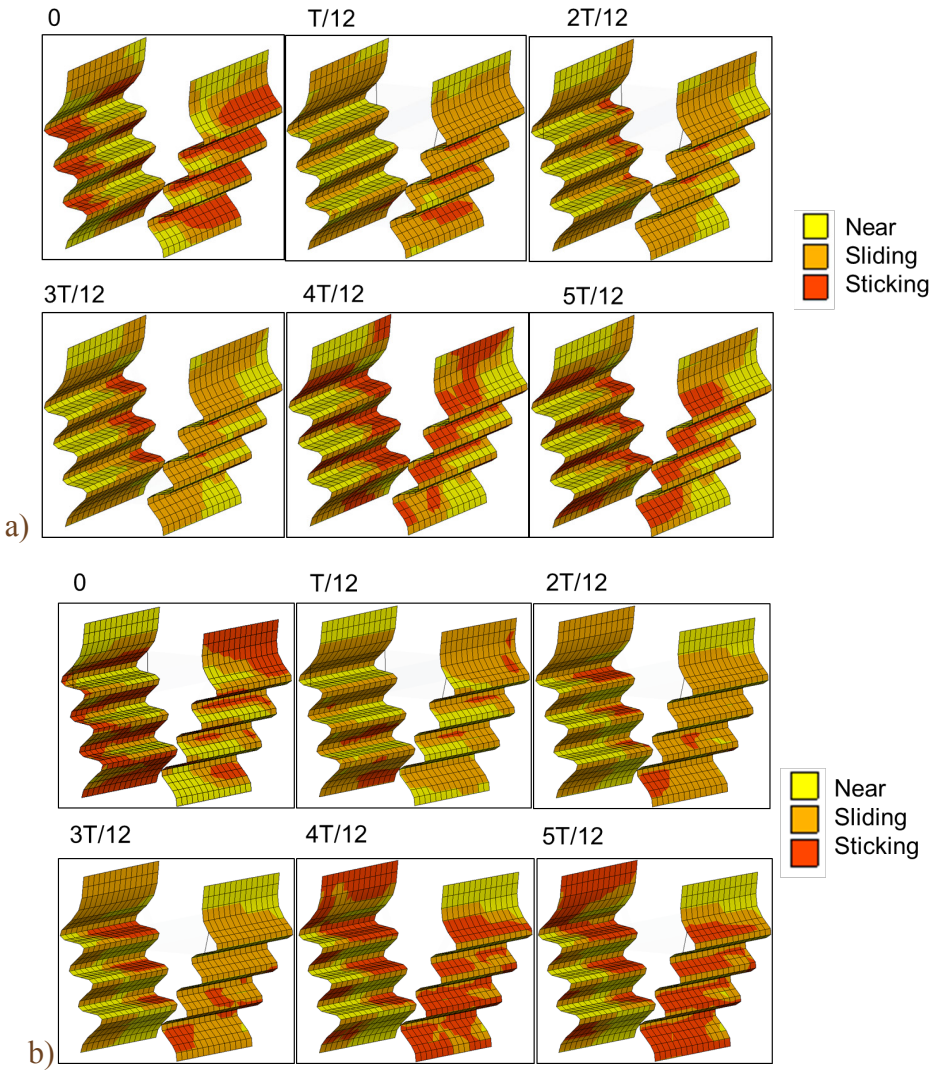

Figure 16. Change of the contact state over contact surfaces over half vibration period for 0.5 mm vibration amplitude: a) 1E mode; b) 2F mode,

Effect of contact parameters

The most commonly considered contact parameters in friction problems are friction coefficient and tangential and normal contact stiffness, and their influence on damping factor is explored here. Figure 17 shows how the damping factor changes with the variation of the friction coefficient from 0.3 to 0.5 for two amplitude levels: (i) 0.01mm and (ii) 0.5mm for all 4 modes.

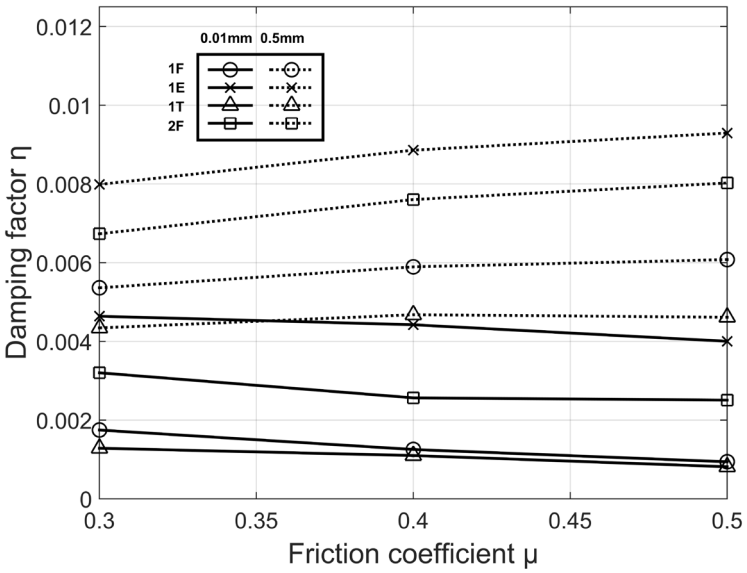

Figure 17. Modal damping factor dependency on the friction coefficient

The amplitude level 0.01mm corresponds to low level of amplitudes, when the major part of the contact area is stuck, because of this; the increase of the friction coefficient reduces the slipping portion of the contact area and then the modal damping decreases for all modes, as we can see in Figure 17. The amplitude level 0.5mm is located after the maximum damping factor on the curves corresponding to all modes in Figure 14 , which indicates that the most of the contact patches are slipping. For this vibration level, the increase of the friction coefficient value increases the friction forces without affecting slipping areas – which leads to the increase of the damping factor.

The effect of coefficients characterising the elastic properties of microasperity layers for rough surfaces on modal damping is illustrated in Figure 18. The dependency of the modal damping factor on the tangential, k_t, and normal, k_n, contact stiffness values is shown for the case when blade tip amplitude is 0.05mm in 2F mode.

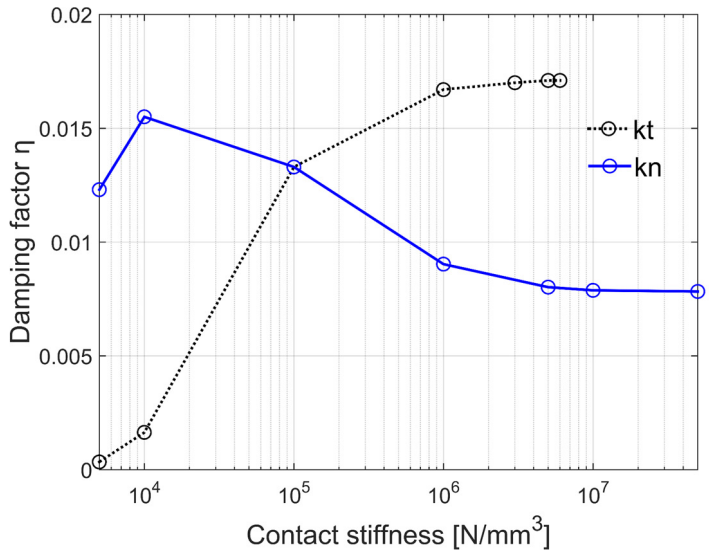

Figure 18. Effect of contact tangential and normal stiffness coefficients on the modal damping

Each of the stiffness coefficients is varied independently from value 5000 to 10^7. During this variation of one of these two stiffness coefficients, the value of the other is kept constant and equal to 10^5. Analysis of the results shows that, for the small values of the tangential stiffness, very large relative displacements are required to cause slip and, therefore, the stick state exists over the whole contact area for such stiffness values. The elastic deformation at the stick state does not dissipate the energy and the very small damping is observed for small values of the tangential stiffness. With the increase of the tangential stiffness, the tangential force can reach the friction limiting level at some contact patches and slip and the dissipation of the energy appears. Further increase of the tangential contact stiffness makes it comparable with the stiffness of the bulk material adjoined to the contact interface and, for sufficiently large values, the particular choice of the tangential and normal stiffness and values does not affect the damping factor. With the increase of normal contact stiffness, the damping factor increases at first, after that it has the tendency to decrease.

The increase of the normal contact stiffness is less significant for its low values than the tangential stiffness in the considered blade root configuration. The normal stiffness value variation can change distribution of the contact pressure and the contribution of the dynamic component in the total contact pressure, which is a sum of static and dynamic components of pressure.

Effect of rotating speed

The influence of rotating speed on damping factor for different mode shapes is shown in Figure 19. The amplitude of the tip in calculation with first four mode shapes is 0.05mm. Rotating speed is varied within range 300...1000 rad/s. One can that different mode affected by the rotation speed variation in rather different ways. For the considered mode and vibration level, the modal damping is reached it maximum at practically the same rotation speed, 800rad/s, for modes 1T, 1E, 2F. Yet, the rotation speed variation changes significantly the ratio between modal damping factor values for the considered four modes, e.g. at 300 rad/s mode 1T has the minimum modal damping factor and at 1000rad/s mode 1F has the minimum damping factors from the four considered here.

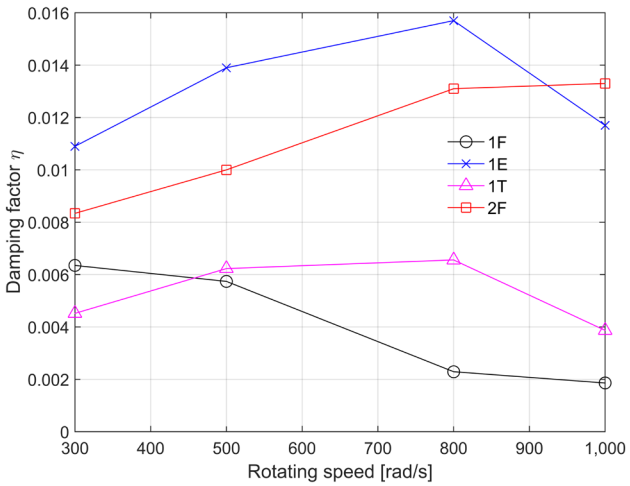

Figure 19. Variation of the modal damping factor with rotating speed change

A realistic bladed disc

A compressor bladed disc, comprising 86 sectors shown in Figure 2 is analysed. The FE model used to calculate the nodal displacements for different mode shapes is shown in Figure 2b. The whole bladed disc model contains 5.6 millions DOFs, and its sector model comprises about 66 thousands DOFs. The natural frequencies and mode shapes of this bladed disc are obtained using the sector model for nodal diameters (ND) from 0 to 24. The dependencies of natural frequencies on the number of nodal diameters are plotted for first four natural frequencies in Figure 20. The bladed disc operating at a rotation speed 1000rad/s, and blade root model shown in Figure 2c is analysed with the accounting for the interaction of the root joint with the rest part of the whole bladed disc model using the developed method. The example of first four mode shapes analysed are plotted in Figure 21 for a cases of 2ND and 24ND. It should be noted that for 24ND the mode shapes are bladed-dominated, are close to the mode shapes of the single blade considered above and can be classified with the conventional classification 1F, 1E, 1T and 2F. For 2ND modes the disk participates significantly in the vibration and such classification is avoided for all low ND numbers considered in this section. Because of this, the modes are indicated simply by their order in the spectrum of natural frequencies in further plots.

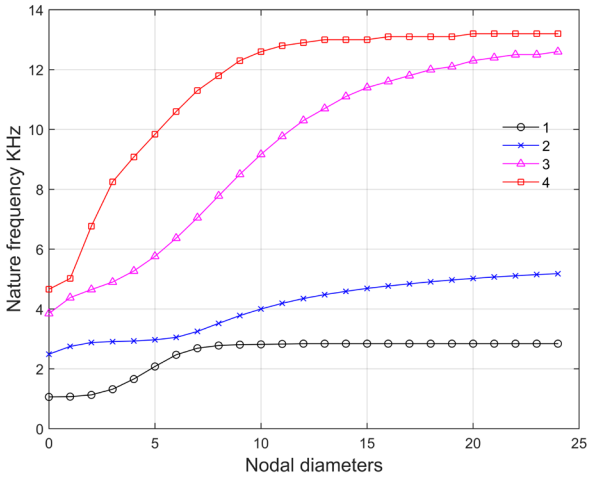

Figure 20. Natural frequencies of the tuned bladed disc

a)

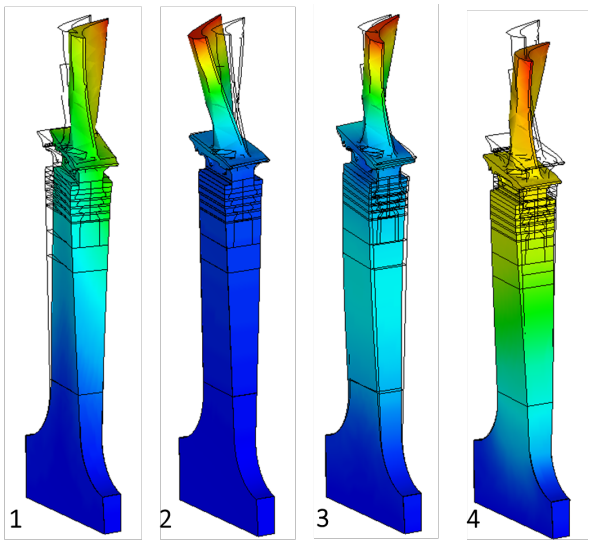

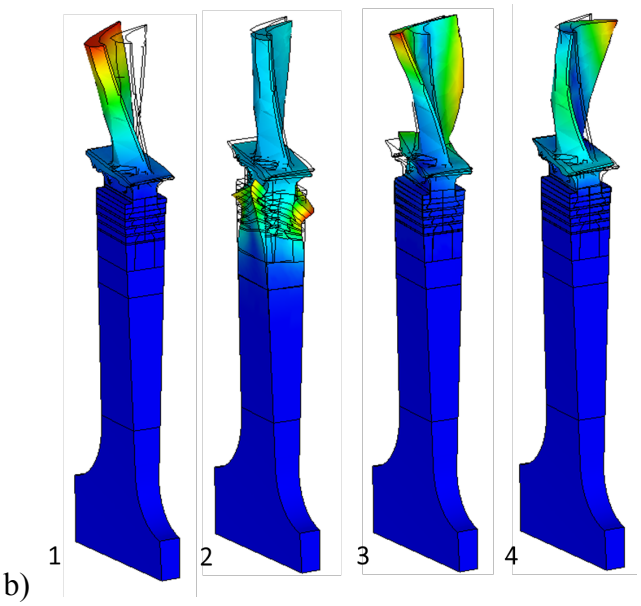

Figure 21. First 4 bladed disk modes: a) 2ND mode shapes; b) 24ND mode shapes: 1F, 1E, 1T, 2F

In this paper, the examples of modal damping calculation are presented for cases of modes families with 0, 2 and 24 NDs. The non-zero ND numbers the mode shapes are excited by the travelling wave engine order excitation (EO) and, because the bladed disc is tuned, this excitation excites the traveling mode shapes with the number of diameters corresponding to the number of EOs.

Effect of vibration amplitude

The mode shapes corresponding to travelling wave mode shapes have real and imaginary parts, which reflect the phase shift between displacements at different locations. Moreover, the different coordinate components, x, y, and z of displacements at each node can have phase shift too. Because of this, we calculate the maximum magnitude of displacement vector at a node: $a = \max_{0 \le t \le T} \sqrt{x^2(t) + y^2(t) + z^2(t)}$ to characterise the vibration levels.

The dependency of the modal damping factor on the amplitude is plotted in Figure 22, Figure 23, and Figure 24, for 0, 2 and 24ND families of modes respectively. The blade tip amplitudes variation range from 0.05 to 1mm is considered. One can see that the modal damping factors increase with the amplitude increase in the amplitude range from 0.05 to 0.3 mm for all considered here NDs. With further increase of the blade tip amplitudes different modes for different NDs can exhibit different behaviour.

For the first family of modes for all considered here NDs the modal damping continues to rise with the increased rate of modal damping increase with the amplitude increase. For 4th family of modes the modal damping decreases with the different rate of decrease with the amplitude change: sharp decrease for 0ND and 2ND and very small decrease for 24ND. For 2nd and 3rd modes excited by 24ND the modal damping is also slow decreased with the increase of amplitudes from 0.3 to

1mm, while for 0ND these modes have the highest damping at the amplitude level 0.7 mm.

It is evident also that the damping produced at blade root by friction is much higher for modes of 24ND than to the other ND numbers considered here. This can be attributed to the fact that for modes excited by 0ND and 2ND the disc is significantly involved in the vibrations and contributes significantly to the blade tip motion, which is used here as the amplitude control parameter in the horizontal scale of the plots. The friction damping is dependent on the relative motion at the blade root and for modes excited by 24ND the ratio between blade tip amplitude and the motion at blade root is significantly smaller than those excited by 0ND and 2ND.

The difference between the damping factors corresponding to different mode shapes can be also in some cases attributed to different ratio between amplitudes at blade tips and at blade root joints. For example, for the same level of blade tip amplitude, the displacement at the surface where the blade body is attached to the blade root joint model is larger for 2F mode approximately by factor of 4 than the displacement for 1F mode. Because of this for 2F mode (mode 2 in Figure 24) much higher friction damping is observed than for 1F mode (mode 1 in Figure 24).

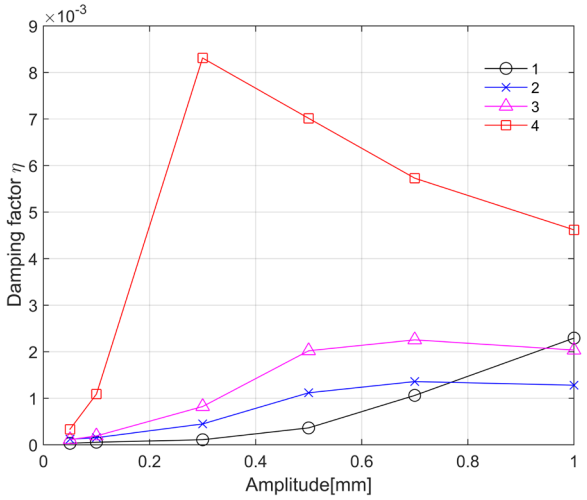

Figure 22. Dependency of the modal damping on the amplitude: 0ND modes

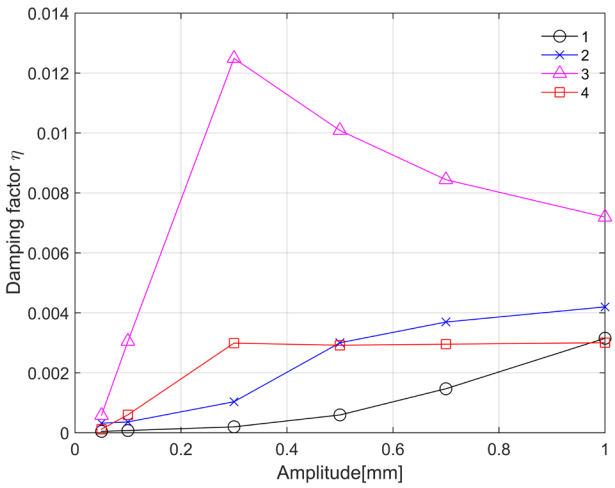

Figure 23. Dependency of the modal damping on the amplitude: 2ND modes

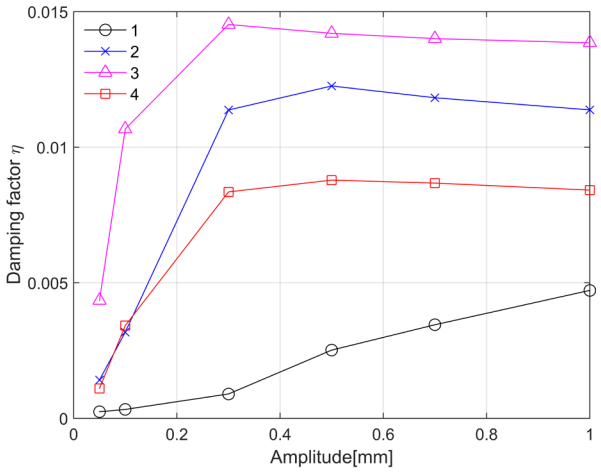

Figure 24. Dependency of the modal damping on the amplitude: 24ND modes

The modal damping factors for 1E and 1T are significantly larger than 1F and 2F ant the ratios between modal factors for different modes differs from those for a single blade considered earlier.

Effect of contact parameters

The dependencies of the damping factor on friction coefficient and contact stiffness are shown in Figure 25 for blade-dominated family of modes: 24ND.

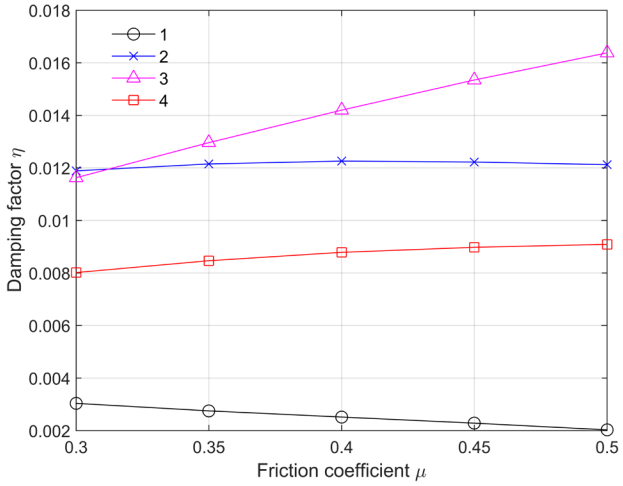

Figure 25. Effect of the friction coefficient variation on modal damping factor

Amplitudes 0.5mm for four mode shapes are used in these examples. The damping factor for 1F mode decreases when friction coefficient increases, even it is with a very low value, while for other modes the tendency is opposite.

In Figure 26, the damping factor variation is shown with the tangential and normal contact stiffness variation. A case of 0.5mm vibration amplitude level and 1E mode are considered here. This behaviour here is similar to what we observed in the analysis of the single blade (see Figure 18). We can see that when the stiffness

coefficient value is large enough, the influence of normal contact stiffness on damping for blade root become negligible. Moreover, for the bladed disc the effect of contact stiffness is smaller than for the single blade analysis.

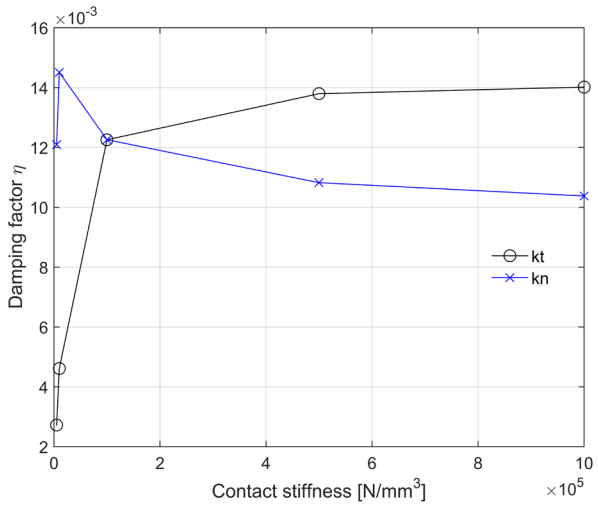

Figure 26. Dependency of modal damping on contact stiffness coefficients: 24ND, 1E mode

CONCLUSIONS

A generic method for analysis of modal damping generated by micro-slip friction at blade-disc root joints has been developed. The method applies the high-fidelity models of bladed discs with friction contact interfaces and takes into account nonlinear interactions at the contact surfaces. The method performs the nonlinear vibration analysis in time domain and allows using widely available commercial finite element packages.

An effective model reduction technique is proposed which allows the transient response calculations to be performed for a small part of the whole disc model: that which includes the friction joints. The interaction of the selected part with the whole disc model is modelled with high accuracy. The model reduction is based on the assumption that the analysed mode shape at the boundaries of the selected part is not affected significantly by the friction interactions at the blade root contact surfaces. The energy dissipated at all contact interfaces is calculated by direct evaluation of the work of the friction stresses over all contact interface elements.

Numerical studies of the modal damping factors due to friction in blade root joints have been performed on large-scale three-dimensional finite element models with root joints: (i) a simplified blade model; (ii) a single realistic blade, and (iii) a realistic tuned bladed disc containing 86 blades. The tuned bladed disc analysis can be performed for travelling wave mode shapes of any nodal diameter and mode shape numbers using the cyclic symmetry properties and bladed disc sector model.

The dependencies of modal damping factors on the vibration amplitudes for different mode shapes (1F, 1T, 1E and 2F modes are considered), on contact interface parameters (friction and contact stiffness coefficients) and on the static preloading due to centrifugal forces in a rotating bladed disc are studied.

The proposed method provides an effective and useful tool for modal damping factor prediction for vibrations with different blade mode shapes for bladed discs with friction damping at root joints.

Acknowledgement

This work was supported in part by the National Natural Science Foundation of China (Project No. 11372128), and NSAF (Project No.U1730129), the Natural Science Foundation of Jiangsu Province (No. BK20161485) and Jiangsu Province Key Laboratory of Aerospace Power System (No. NJ20160019). The supports by the Collaborative Innovation Center of Advanced Aero-Engine, the Key Laboratory of Aero-engine Thermal Environment and Structure, Ministry of Industry and Information Technology are also gratefully acknowledged.

References

1. Firrone, C.M., Zucca, S. and Gola, M.M., "The effect of underplatform dampers on the forced response of bladed disks by a coupled static/dynamic harmonic balance method", Int. J. of Non-Linear Mechanics, 2011, 46(2), pp. 363-375

2. Petrov, E.P., "Explicit Finite Element Models of Friction Dampers in Forced Response Analysis of Bladed Disks", J. of Eng. for Gas Turbines & Power, 2007, 130(2), pp. 277-285

3. Meguid, S.A., Refaat, M.H. and Papanikos, P., "Theoretical and experimental studies of structural integrity of dovetail joints in aeroengine discs", J. of Materials Processing Technology, 1996, 56(1–4), pp. 668-677

4. Papanikos, P., Meguid, S.A. and Stjepanovic, Z., "Three-dimensional nonlinear finite element analysis of dovetail joints in aeroengine discs", Finite Elements in Analysis and Design, 1998, 29, pp. 173-186

5. Marquina, F.J., Coro, A., Gutiérrez A, et al., "Friction Damping Modeling in High Stress Contact Areas Using Microslip Friction Model", Proc. of ASME Turbo Expo 2008 June 9-13, 2008, Berlin, Germany, GT2008-50359

6. Petrov, E.P. and Ewins, D.J., "Analysis of essentially non-linear vibration of large-scale models for bladed discs with variable contact and friction at root joints", Proc. of the 8th Int. Conference on Vibrations in Rotating Machinery, Sep 07-09, 2004, Swansea, UK

7. Charleux, D., Thouverez, F. and Lombard, J.P., “Three dimensional multi harmonic analysis of contact and friction in dovetail joints”, Proc. of the 22nd Int. Modal Analysis Conference, 2004, Detroit, Michigan, USA

8. Petrov, E.P., Ewins, D.J., “Effects of Damping and Varying Contact Area at Blade-Disk Joints in Forced Response Analysis of Bladed Disk Assemblies”, J. of Turbomachinery, 2006, 128(128), pp. 403-410

9. Charleux, D., Gibert, C., Thouverez, F., et al., “Numerical and Experimental Study of Friction Damping Blade Attachments of Rotating Bladed Disks”, Int. J. of Rotating Machinery, 2006, 2006, pp.1-13.

10. Shangguan B., Yu F., Duan J., et al., “A Fractal Contact Friction Model and Nonlinear Vibration Response Studies of Loosely Assembled Blade With Dovetail Root”, Proc. of ASME Turbo Expo 2016, June 13–17, 2016, Seoul, South Korea, GT2016-56271

11. Hong J., Chen L., Ma Y., et al., “Design Methods of Friction Damping at Blade-Disk Joints”, Proc. of ASME Turbo Expo 2009, June 8-12, 2009, Orlando, Florida, USA, GT2009-59510

12. Allara, M., Filippi, S., Gola, M.M., “An Experimental Method for the Measurement of Blade-Root Damping”, Proc. of ASME Turbo Expo 2006, May 8-11, 2006, Barcelona, Spain, GT2006-90774

13. Firrone, C.M., Bertino, I., “Experimental Investigation on the Damping Effectiveness of Blade Root Joints”, Experimental Mechanics,2015, 55(5), pp. 1-8

14. Zucca, S., Gola, M., Firrone, C.M., “A Method for the Calculation of Friction Damping in Blade Root Joints”, Proc. of ASME 2010, Biennial Conference on Engineering Systems Design and Analysis, July 12-14, 2010, Istanbul, Turkey, ESDA2010-24948

15. Chen J., Zang C., Zhou B., Petrov, E., “A study of friction microslip modeling for dynamic analysis of bladed discs with root joints”, Proc. of the Institution of Mechanical Engineers, Part C: J. of Mech. Eng. Science

16. Petrov, E., “A high-accuracy model reduction for analysis of nonlinear vibrations in structures with contact interfaces”, Trans. ASME: J. of Eng. for Gas Turbines and Power, Oct 2011, Vol.133, 102503

17. Zucca, S., Epureanu, B.I., “Bi-linear reduced-order models of structures with friction intermittent contacts”, Nonlinear Dynamics, 77 (3) (2014) 1055–1067

18. Schwingshackl, C.W., Natoli, A., “Explicit modelling of microslip behaviour in dry friction contact”, Proc. of 34th IMAC Conference and Exposition on Structural Dynamics, Publisher, 2016, 4, pp. 265-272

19. Schwingshackl, C.W., Petrov, E.P. and Ewins, D.J., “Measured and estimated friction interface parameters in a nonlinear dynamic analysis”, Mechanical Systems & Signal Processing, 28(2), pp. 574–584, 2012

20. Toupin, R.A., “Saint-Venant’s Principle”, Archive for Rational Mech. and Anal., 18 (1965), 83-96

21. Berdichevskii, V.L., “On the proof of the Saint-Venant Principle for bodies of arbitrary shape”, Appl. Math, and Mech., Vol. 38, no.5, 1974, p. 799-813.